Food Chemistry: X 23 (2024) 101778

Contents lists available at ScienceDirect

Food Chemistry: X

journal homepage: www.sciencedirect.com/journal/food-chemistry-x

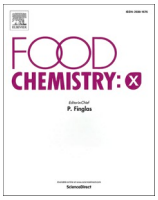

Structural characterization and antioxidant activities of polysaccharides extracted from Polygonati rhizoma pomace

Yunke Bu [a,b], Bangfeng Yin [b], Zhichang Qiu [c], Lingyu Li [b], Bin Zhang [b], Zhenjia Zheng [b,*], Minmin Li [a,*]

[a] Key Laboratory of Agro-products Quality and Safety Control in Storage and Transport Process, Ministry of Agriculture and Rural Affairs/Institute of Food Science and Technology, Chinese Academy of Agricultural Sciences, Beijing 100193, PR China
[b] Key Laboratory of Food Nutrition and Health in Universities of Shandong, College of Food Science and Engineering, Shandong Agricultural University, 61 Daizong Street, Tai'an, Shandong 271018, PR China
[c] Department of Food Science, University of Massachusetts, Amherst, MA 01003, United States

ARTICLE INFO

Keywords:
Polygonatum rhizome pomace
Polysaccharide extraction
Structural characterization
Antioxidant activity
Waste valorization

ABSTRACT

The present study aimed to prepare polysaccharides from the pomace of *Polygonatum* rhizome and characterize their structural features and biological activities. After hot water extraction and DEAE-52 cellulose fractionation, a neutral polysaccharide (PKP) was obtained with 91.85% sugars and 0.45% proteins. Structural characterization indicated that PKP contained a main fraction with a molecular weight of 4.634×10^3 Da and was composed of →1)-*β*-D-Fru*f*-(2→ and →6)-*β*-D-Fru*f*-(2→ residues. PKP was a semi-crystalline polymer, and the Congo red assay suggested the presence of triple-helix structure in PKP. PKP exhibited moderate radical scavenging activity (including 15.55% inhibition of DPPH, 21.48% inhibition of ABTS, and 22.52% inhibition of ·OH) and could effectively protect MRC-5 cells from H_2O_2-induced oxidative damage at 0.01 mg/mL through inhibiting apoptosis, decreasing SA-*β*-galactosidase activity, and downregulating the expression levels of p16 and p53. Therefore, PKP could be used in functional foods and pharmaceuticals as an antioxidant. This study provides an attractive method for utilizing polysaccharides from waste materials.

1. Introduction

"Huangjing" or "Yuzhu" belongs to the genus *Polygonatum* of *Asparagaceae* family and has been used as a vegetable and herb for centuries. The genus *Polygonatum* is rich in bioactive components, including saponins, flavonoids, alkaloids, polysaccharides, vitamins, amino acids, and lignans (Pan et al., 2024). These nutrients confer a variety of pharmacological effects and health benefits (*e.g.*, anti-aging, immunostimulatory, antioxidant, anti-inflammatory, and hypolipidemic properties) and support the development and application of the genus *Polygonatum* in health food products (Pan et al., 2024).

Polysaccharides are a class of biomacromolecular polymers linked by glycosidic linkages and are one of the main components responsible for the functional properties of the genus *Polygonatum* (Pan et al., 2024). Nowadays, there is a growing interest in natural plant polysaccharides with the increasing awareness of diet-health relationships, and a series of polysaccharides have been produced, structurally characterized, and applied in functional foods using different *Polygonatum* species as materials. Wang and coworkers prepared a polysaccharide from *P. sibiricum via* water extraction and purification with column chromatography, with a structure mainly composed of →1)-*β*-D-Fru*f*-(2→, →6)-*β*-D-Fru*f*-(2→, →4)-*β*-D-Man*p*-(1→, and →6)-*β*-D-Glc*p*-(1→ (Wang et al., 2022). This polysaccharide could effectively scavenge radicals (including 2,2-diphenyl-1-picrylhydrazyl (DPPH), ·OH and $\cdot O^{2-}$) and chelate ferrous ions (Wang et al., 2022). Using a similar production procedure of water extraction and column purification, Zhang et al. (2021) obtained a fructan composed of a (2 → 6) linked-*β*-D-Fru*f* backbone from *P. cyrtonema* and a galactan consisting of a (1 → 4)-*β*-D-Gal*p* chain from processed *P. cyrtonema* (Nine-Steam-Nine-Bask). These two polysaccharides showed excellent prebiotic activity by expanding *Bifidobacterium* and *Lactobacillus* strains. In another study, a hypoglycemic polysaccharide (PKPs-1) from *P. kingianum* was reported to contain →2)-Glc*p*-(1→, →6)-Glc*p*-(1→, →2)-Man*p*-(1→, and →4)-Glc*p*-(1→, as well as terminal T-Glc*p*-(1→. PKPs-1 showed great potential in managing type 1 diabetes as functional supplements through improving insulin tolerance (PI3K/AKT signaling pathway) and affecting serum

* Corresponding authors.
E-mail addresses: zhengzhenjia@sdau.edu.cn (Z. Zheng), liminmin@caas.cn (M. Li).

https://doi.org/10.1016/j.fochx.2024.101778
Received 1 July 2024; Received in revised form 22 August 2024; Accepted 24 August 2024
Available online 26 August 2024
2590-1575/© 2024 Published by Elsevier Ltd. This is an open access article under the CC BY-NC-ND license (http://creativecommons.org/licenses/by-nc-nd/4.0/).

lipid metabolism (Li et al., 2020). Furthermore, there are other polysaccharides with different structures (linear or branched) and biological activities (anti-diabetic, immuno-modulatory, antitumor, anti-osteoporosis) from the genus *Polygonatum* (Hu et al., 2023). Previous research on polysaccharides from the genus *Polygonatum* has focused on raw and processed rhizomes (after the "Nine-Steam-Nine-Bask" process), but polysaccharides from *Polygonatum* rhizome pomace (wastes and by-products from the extraction of flavonoids and saponins) have not yet been well understood or extensively reported. The variety and handling methods of materials, extraction techniques, and molecular modifications have been shown to significantly affect the structure and function of the obtained polysaccharides (Lu, 2023; Qiu, Qiao, Zhang, Sun-Waterhouse, & Zheng, 2022). Therefore, it is of high interest to extract polysaccharides from *Polygonatum* rhizome pomace and examine their structural and functional properties.

This study aimed to fill these knowledge gaps. Polysaccharides were extracted from *Polygonatum* rhizome pomace *via* hot water diffusion. Hot water extraction is the most commonly employed method for producing plant polysaccharides according to the principle of "similar compatibility" (polar macromolecular polysaccharides are dissolved in polar solvents such as water) (Lu, 2023; Zeng, Li, Chen, & Zhang, 2019). This method has the advantages of simple operation, low cost, high safety, and minimal pollution. The obtained crude polysaccharides were further purified and fractionated based on chromatographic columns. Their structural features were examined by various spectroscopic and chromatographic techniques. Finally, the antioxidant activities of polysaccharides were evaluated based on chemical assays and H_2O_2-damaged MRC-5 fibroblasts. The results are expected to provide in-depth insights into the feasibility of producing bioactive polysaccharides from *Polygonatum* rhizome pomace as a novel antioxidant.

2. Materials and methods

2.1. Materials and chemicals

Dried roots of *P. kingianum* and its by-products were collected from Wenshan city, Yunan province, China. DEAE-52 cellulose, DPPH, and 2, 2′-azinobis-3-ethylbenzotiazo-line-6-sulfonic acid (ABTS) were purchased from Yuanye Biotechnology Co., Ltd. (Shanghai, China). The monosaccharide standards, trifluoroacetic acid (TFA), dextran standards, and Congo red were provided by Sigma-Aldrich (St. Louis, MO, USA). All other chemicals and reagents were of analytical grade.

2.2. Production and purification of polysaccharides

Polygonatum rhizome pomace (after the extraction of flavonoids and saponins) was dried at 40 °C and then ground into powder (425 μm) using a Royalstar RS-FS2201 disintegrator (Hefei, China). The production of *Polygonatum* rhizome polysaccharides was performed following the previous procedure with minor modifications based on pilot experiments. *Polygonatum* rhizome polysaccharides were extracted twice at 80 °C for 1.5 h each in a material-distilled water ratio of 1:10 (*w/v*) (Li et al., 2021). The resulting supernatant obtained by centrifugation (8000 *g*, 20 min) was concentrated at 60 °C (to one-fourth of its original volume) and precipitated with absolute ethanol (final concentration of polysaccharide-ethanol mixtures: 80%, *v/v*) for 12 h. The precipitate (*i.e.*, crude polysaccharides) was redissolved into an aqueous solution and deproteinized with a chloroform/*n*-butanol mixture (4:1, *v/v*) in a polysaccharide juice-organic solvent ratio of 1:4 (*v/v*), before fractionation using a DEAE-52 cellulose column (6.0 × 100.0 cm) (Qi et al., 2023). The elution was performed sequentially using distilled water and different aqueous sodium chloride solutions at 25 °C. According to the results from the Phenol-sulfuric acid assay, the same fractions were combined, rotary evaporated at 60 °C, and dialyzed with dialysis membranes (500–1000 Da) at 4 °C. These individual samples were freeze-dried and stored in sealed tubes in a desiccator for further analysis.

2.3. Chemical composition of polysaccharides

The purity and chemical composition of the samples were analyzed based on total sugar content (Phenol-sulfuric acid method), as well as uronic acid content (*m*-hydroxydiphenyl method) and protein content (Bradford method) (Han et al., 2016).

2.4. Molecular weight distribution and monosaccharide profile

The polysaccharide samples were dissolved into a 2 mg/mL aqueous solution and purified using a 0.45 μm syringe filter, before injection into a high-performance gel permeation chromatography coupled with multi-angle laser light scattering and refractive index detector (HPGPC-MALLS/RID, Wyatt-DAWN HELEOS-II, USA). A Shodex SB-806 HQ size-exclusion column was used to elute samples using 0.1 mol/L aqueous sodium chloride solution at 0.5 mL/min. The polysaccharide samples were placed in an ampoule and then hydrolyzed with 2.0 mol/L TFA under previously optimized conditions (Li et al., 2021). After the removal of excess TFA, the monosaccharide units in the hydrolysate were eluted using a Dionex™ ICS-5000$^+$ high-performance anion-exchange chromatography (HPAEC) system along with a Dionex™ CarboPac™ PA20 IC chromatography column (3 × 150 mm, Thermo Fisher Scientific, USA). The flow rate and column temperature were kept at 0.25 mL/min and 30 °C, respectively. The separated monosaccharides were detected using a pulsed amperometric detector (PAD).

2.5. Ultraviolet-visible (UV–vis) and Fourier transform infrared (FTIR) spectra

The UV–vis spectra of aqueous polysaccharide solutions over a range of 200–800 nm were determined using quartz cuvettes in a UV-2450 spectrophotometer (Shimadzu, Japan). In terms of FTIR spectra, the dried polysaccharide powder was scanned directly on an accessory plate using a Thermo Scientific Nicolet iS10 FTIR spectrometer (Madison, USA) in the range of 4000–400 cm^{-1}. The obtained spectra were processed using OMNIC 8.2.0.387 software and annotated with functional groups.

2.6. Microscopic analysis, particle size and zeta potential

The dried polysaccharide particles were deposited onto the sample stage and sputtered with gold, before their morphological features were observed and recorded using a Zeiss-SUPRATM 55 scanning electron microscope (SEM, Oberkochen, Germany). The acceleration voltage was set to 5 kV under high vacuum conditions. The polysaccharide samples were prepared as an aqueous solution of 1.0 mg/mL, and then the particle size and zeta potential were measured using a Zetasizer Nano ZS laser nanometer particle size analyzer (Malvern, Worcestershire, UK).

2.7. X-ray diffraction (XRD) pattern and helix-coil transition assay

XRD patterns of polysaccharide samples were determined in the diffraction angle (2θ) range of 5°–80° using an EMPYREAN X-ray diffractometer equipped with a Cu Kα radiation source (Panalytical B.V., Almelo, Netherlands). The polysaccharide solution (2.5 mg/mL) and an equal volume of Congo red solution (80 μmol/L, 2.0 mL) were mixed in a conical flask, and then NaOH solution was added to a final concentration of 0.05–0.50 mol/L. The maximum absorption wavelengths of the above solutions were recorded using a UV-2450 spectrophotometer (Shimadzu, Japan).

2.8. Methylation analysis and nuclear magnetic resonance (NMR) spectra

The glycosidic linkage patterns of polysaccharides were determined by methylation analysis following previously published procedures (Liu, Qiu, Gu, Wang, & Zhang, 2023). The polysaccharide samples were subjected to reduction, methylation, hydrolysis, re-reduction, and derivatization. The obtained monosaccharide derivatives were determined using an Agilent 7820 A-5977 gas chromatograph-mass spectrometer equipped with an Agilent 5977B electron impact ion trap MS detector (Santa Clara, CA, USA). In terms of NMR spectra, 30.0 mg of the dried polysaccharide sample was completely dissolved in D_2O and purified with an MCE membrane filter (0.45 μm) prior to loading into an NMR tube. A AVANCE III 600 NMR spectrometer (Bruker, Germany) was used to determine one-dimensional NMR spectra and two-dimensional NMR spectra of the samples.

2.9. Antioxidant activity

2.9.1. Chemical assays

The polysaccharides were prepared as a 1.0 mg/mL aqueous solution. The scavenging activities against DPPH, ABTS, and ·OH radicals were determined following the methods of Tang et al. (2023) and Yuan, Qiu, Yang, Liu, and Zhang (2022). Briefly, DPPH radical scavenging activity was assessed by incubating 0.5 mL of polysaccharide solution and 3.5 mL of DPPH solution (100 μmol/L in absolute ethanol) for 30 min in the dark and then determining the decrease in absorbance at 517 nm. For ABTS radical scavenging activity, the mixture of 7.4 mmol/L ABTS solution and 2.6 mmol/L potassium persulphate solution (1:1, *v/v*) was pre-reacted for 12 h in the dark and adjusted with phosphate buffer (pH 7.4) to an absorbance of 0.7 at 734 nm. Then, 0.2 mL of the polysaccharide solution and 0.8 mL of the ABTS working solution were incubated for 6 min in the dark and determined for the absorbance at 734 nm. Furthermore, 2 mL of polysaccharide solution was mixed with 2.0 mL of ferrous sulphate solution (8 mmol/L), 2.0 mL of salicylic acid solution (8 mmol/L), and 2.0 mL of hydrogen peroxide solution (8 mmol/L), and incubated at 37 °C for 30 min. The decrease in absorbance of the reaction system was determined at 510 nm to calculate the ·OH radical scavenging activity. The free radical scavenging activity assay was conducted in six replicates, and the results were averaged.

2.9.2. Antioxidant activity based on H_2O_2-treated MRC-5 fibroblasts

MRC-5 cells were cultured at 37 °C in a humidified atmosphere containing 5% CO_2 using minimum essential medium (MEM) supplemented with 10% fetal bovine serum. The activated cells were transferred to 96-well culture plates at a density of 2×10^4 cells per well), and the cytotoxicity of polysaccharides at concentration ranging from 0.01 to 0.8 mg/mL was evaluated using the MTT assay. The polysaccharides that were not significantly toxic to cells were used for the antioxidant activity assay based on cell viability. Then, H_2O_2 concentration was selected through treating MRC-5 cells with different concentration of H_2O_2 (0–700 μmol/L) and monitoring their cell viability.

The protective effects of polysaccharides against oxidative damage were examined using H_2O_2-treated MRC-5 fibroblasts. The activated cells into 96-well plates were divided into the following six groups: control group, model group, resveratrol-treated group (supplemented with 30 μmol/L resveratrol), and polysaccharide-treated groups (supplemented with 0.01, 0.05, and 0.2 mg/mL polysaccharides, respectively). After 24 h of inoculation at 37 °C, the original medium was changed to fresh MEM and cultured for another 4 h. Apart from the control group, cells in all experimental groups were exposed to 200 μmol/L H_2O_2 for 24 h, followed by treatment with 10 μL of 5.0 mg/mL MTT solution for 4 h. The cell viability was calculated based on optical density at 490 nm using a Bio-Tek microplate reader (Bio-Tek Instruments, USA). The trypan blue staining was performed by treating cell suspensions with 0.4% trypan blue solution for 10 min and then fixing them with 4% paraformaldehyde for 30 min at 4 °C. The number of dead cells and the survival rate were calculated by counting 300 cells in each treatment with an inverted microscope. The senescence-associated β-galactosidase activity (SA-β-Gal) of MRC-5 cells was assessed in 24-well culture plates. After pretreatment with polysaccharide solution and damage with H_2O_2, MRC-5 cells were fixed with 3% formaldehyde for 5 min at 25 °C and washed three times with phosphate buffered saline. Then, all cells were incubated with β-galactosidase dye in a 37 °C incubator for 12 h, and β-Gal-positive cells displaying bluish colour were observed and counted using an inverted microscope. The protein expression levels of p16 and p53 (key indicators for aging and oxidative damage) were evaluated using western blot following our previous procedure (Liu et al., 2023; Liu, Qiu, et al., 2023).

2.10. Statistical analysis

All results are expressed as "mean ± standard deviation". Statistical significance was evaluated using one-way analysis of variance combined with Duncan's test, performed with SPSS statistical software (*version 28.0*; $P < 0.05$ and 0.01).

3. Results and discussion

3.1. Extraction and purification of polysaccharides

The roots of *P. kingianum* have been extensively used for the extraction of flavonoids and saponins, but the residues pose a huge challenge to resource utilization and environmental burden. In the present study, polysaccharides were isolated from *P. kingianum* pomace using a hot water extraction method and purified using a DEAE-52 cellulose column. The yield of crude polysaccharides was 4.42% (*w/w*), which was comparable to the data obtained by Bai et al. (2021). This suggested a great potential for utilizing this waste material as a polysaccharide resource. As shown in Fig. 1A, neutral polysaccharides (PKP) were the predominant polysaccharide fractions and were thus selected for further structural characterization and bioactivity analysis. Such a result was also observed in a study by Li et al. (2020): The polysaccharides extracted from *P. kingianum* with distilled water at 80 °C showed two independent peaks on a DEAE-Sepharose-FF column, with the water-eluted polysaccharides being dominant. PKP exhibited a total sugar content of 91.85% (*w/w*) and a protein content of 0.45% (*w/w*) and contained no uronic acids. UV–vis spectrum in Fig. 1B suggested that there were no proteins and nucleic acids in PKP.

3.2. Molecular weight distribution and monosaccharide profile

Fig. 1C showed that two peaks appeared in the chromatogram of PKP. The second peak was the most dominant one (with a proportion of 96.20%) and corresponded to a weight-average molecular weight (Mw) of 4.63×10^3 Da. In contrast, the first peak accounted for only 3.80% and had a Mw of 8.57×10^4 Da. Yang and coworkers reported that the Mw distribution of the crude polysaccharides from the roots of *P. kingianum* using hot water extraction method was mainly concentrated in 50–650 kDa (Yang, Zhang, Dai, Ma, & Jiang, 2023). In another study, a purified polysaccharide (PKPs-1) with an average molecular weight of 14.05 kDa was produced from *P. kingianum* by hot water extraction, fractionation on a DEAE-Sepharose-FF column, and purification with a Sephadex G100 column (Li et al., 2020). During extraction of flavonoids or saponins, the polysaccharides may undergo some degradation under the effect of ultrasound, with larger polysaccharide molecules breaking down into smaller fragments, thus lowering their Mws. Furthermore, the removal of flavonoids or saponins can adversely affect the stability of the polysaccharides due to their natural interactions (the tissue becomes loose, or the polysaccharide/flavonoid complex is disrupted). Similar results were observed for pectin extracted

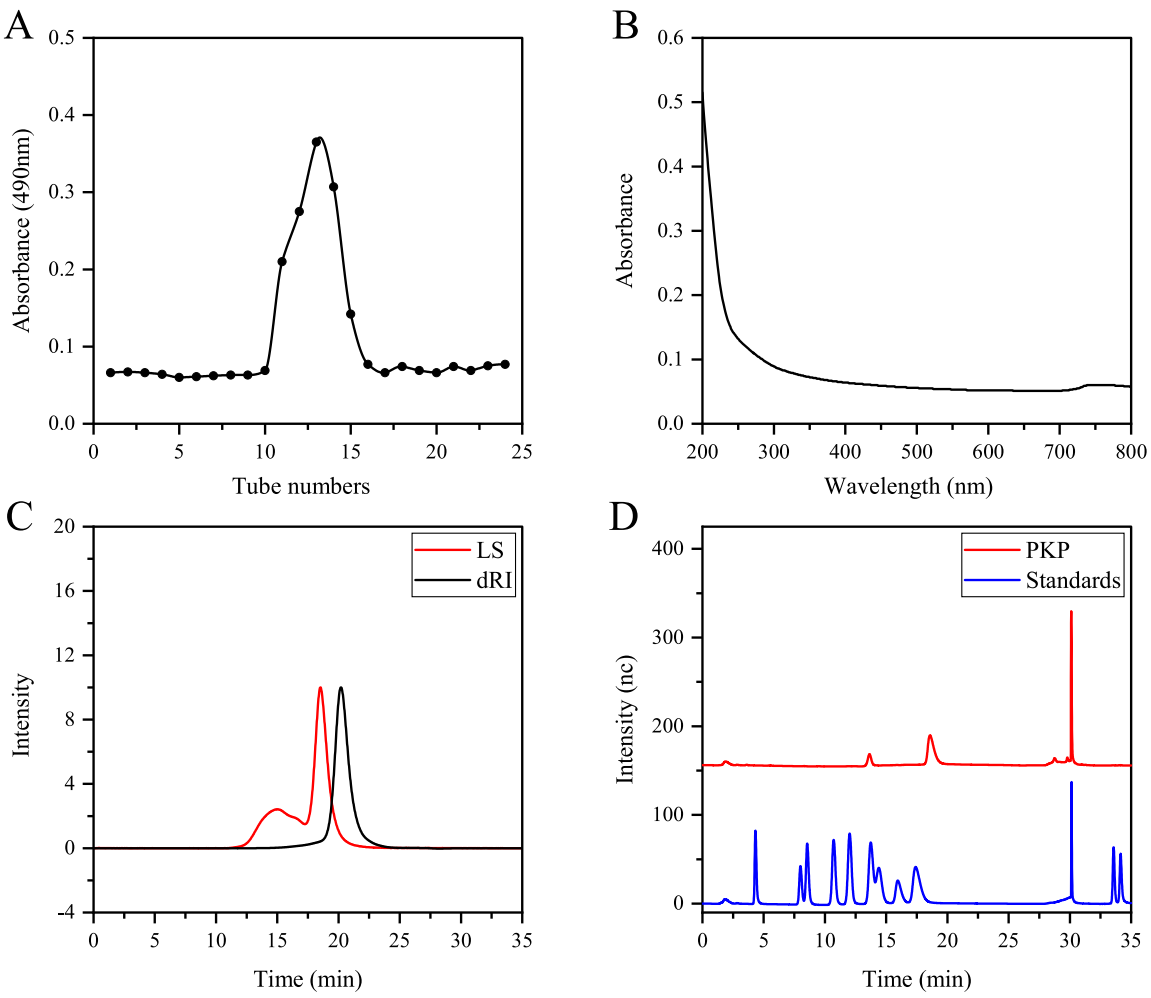

Fig. 1. Elution curve of crude *P. kingianum* polysaccharides (A); UV–vis spectrum (B); molecular weight distribution (C); and monosaccharide composition (D) of the resulting purified neutral polysaccharides (PKP).

from raw garlic and garlic pomace (by-products from the processing of garlic essential oil): The Mw of the pectin decreased from 332.64 kDa to 324.08 kDa (Qiu et al., 2024). Moreover, steaming (one of the traditional herbal processing methods to enhance its function) and fermentation (a promising biological modification method) of *Polygonatum* rhizome were reported to reduce the Mw of contained polysaccharides (Yang et al., 2023; Yu et al., 2024).

As shown in Fig. 1D, PKP consisted of fructose and glucose, and their molar ratio was 93.13: 6.87. Fructose was the most primary monosaccharide unit, about 13.6-fold larger than glucose. This indicated that PKP belonged to fructans. A similar monosaccharide profile was observed in purified polysaccharides from steamed *P. sibiricum*: The constituent units of P1 included fructose and glucose in a molar ratio of 10: 1 (Xu et al., 2023). In a previous study comparing the polysaccharides from three species of *Polygonatum spp.*, a small amount of galactose (14.55%) and galacturonic acid (7.25%) was found in the polysaccharides from *P. kingianum* (Bai et al., 2021). Considering that such polysaccharides were not fractionated by ion exchange chromatographic columns, galactose and galacturonic acid might be derived from the acidic polysaccharide fractions of *P. kingianum*.

3.3. Morphological characteristics, particle size, and zeta potential

At 500 × magnification, PKP appeared like rough, irregular, and thick blocks with numerous holes and cracks on the surface (**Fig. S1**). Under an increased magnification (5000 ×), PKP had relatively smooth surfaces and occurred as interconnected, irregular, extended, and thin "bark" fragment sheets. The morphological characteristics of polysaccharides were closely associated with their structural properties, but also were affected by the production process. The particle size of PKP dispersions was concentrated in the range of 79–220 nm, with an average particle size of about 140 nm, showing a high stability in aqueous solution (Fig. 2A). Furthermore, PKP dispersions had a large negative zeta potential (−16.8 mV). The higher negative zeta potential value of polysaccharides may contribute to their antioxidant activity (Gu et al., 2020).

3.4. FTIR analysis and Congo red assay

As shown in Fig. 2B, the FTIR spectrum of PKP exhibited typical features of plant storage polysaccharides. The IR bands at around 3300 cm^{-1}, 2920 cm^{-1}, and 1640 cm^{-1} were ascribed to the O—H stretching vibrations of hydroxyl groups, C—H stretching vibrations, and antisymmetrical C═O stretching vibrations of free carboxylate groups, respectively (Qiu, Li, Du, et al., 2024; Yuan et al., 2023). The signals observed near 1420 cm^{-1} were associated with C—H deformation vibrations of CH_2/CH_3 groups, O—H bending vibrations or C—O—C asymmetric vibrations. In the fingerprint region of polysaccharides (1200–800 cm^{-1}), the stretching vibrations of O—C—O and C—O—C in the rings and glycosidic linkages and/or C—O—H in the side groups of polysaccharides resulted in signals at 1200–800 cm^{-1} (Qi et al., 2024). The IR bands at 813, 869, and 930 cm^{-1} suggested that there was

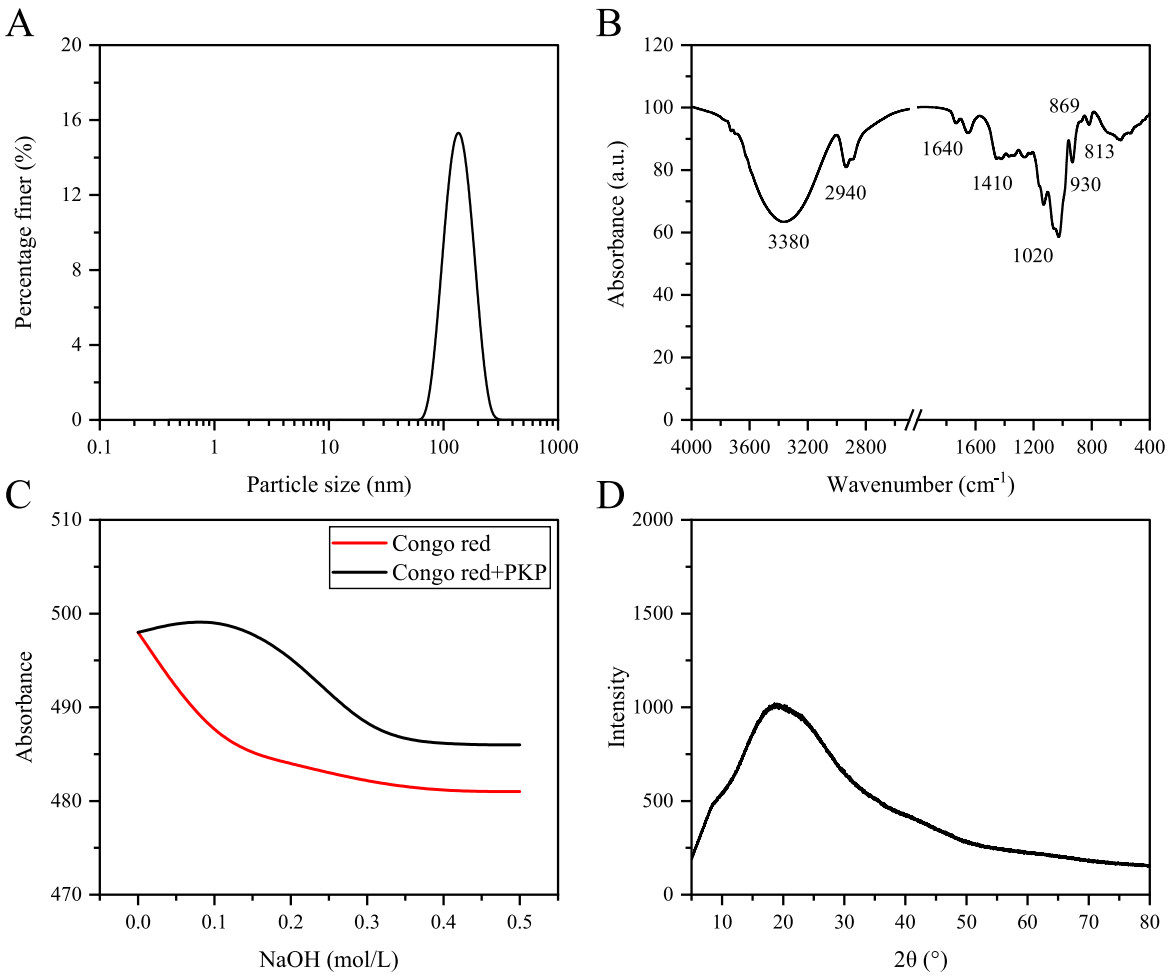

Fig. 2. Structural characterization of PKP. (A) Particle size distribution; (B) FTIR spectrum; (C) Congo red assay; (D) XRD pattern.

abundant fructose with β-configuration glycosidic bonds. This further confirmed that PKP was a fructan. Similar FTIR spectra were observed in the fructans from *P. odoratum*, *P. cyrtonema*, and *Allium sativum* L. (Qiu, Li, Du, et al., 2024; Zhao et al., 2019). Fructans are typical plant storage polysaccharides composed of (2 → 1)-linked β-D-Fru*f* residues and/or (2 → 6)-linked β-D-Fru*f* residues, showing great potential in alleviating oxidative stress, inflammatory responses, and gut microbiota disorders.

The triple-helix conformation is strongly linked to the functional activities and health benefits of polysaccharides, and it can be identified by examining the λ_{max} red shift of Congo red-polysaccharide complexes (containing the triple helical structure)/mixtures (containing no triple helical structure) upon the addition of varying concentrations of alkali solutions (Du, Nie, Peng, Yang, & Xu, 2022). As shown in Fig. 2C, the λmax of the Congo red-polysaccharide system was significantly red-shifted in the presence of 0.1 and 0.2 mol/L of NaOH, compared with the pure Congo red solution. This indicated that PKP underwent a conformational change and had a triple helix conformational state in dilute alkali solution. At the NaOH concentration greater than 0.2 mol/L, the sharp decrease of λmax in the visible spectra could be explained by the disruption of the triple helix (disrupted into single strands of irregular spiral coils) in the high-concentration NaOH solution. The results suggested that PKP had a triple helical structure in aqueous solution. A similar λmax response to NaOH concentration was observed for polysaccharides prepared from *Sagittaria sagittifolia* L. by ultrasound-assisted and subcritical water extraction, but not occurred for those prepared by hot water infusion (Gu et al., 2020). Therefore, the production process significant influenced the chemical structure of the obtained polysaccharides.

3.5. XRD analysis

As shown in Fig. 2D, PKP exhibited a broad diffraction peak at 2θ 19.20° and was thus identified as a semi-crystalline polymer. Compared with the typical crystalline structure of cotton cellulose, there was a relatively low degree of crystallinity in PKP (Nam, French, Condon, & Concha, 2016). Such characteristic XRD pattern was similar to polysaccharides prepared from fresh garlic and *Polygonatum sibiricum*, which also demonstrated typical broad peaks of semi-crystalline structures (Bian, Li, Peng, Wang, & Zhu, 2022; Song et al., 2023). The crystalline state of polysaccharides was determined by their chemical structures. Factors such as monosaccharide profile, glycosidic linkages, and degree of branching greatly affect the packing of polymer chains. In PKP, low crystallinity might be attributed to irregularities in the chain structure, such as the presence of branching or amorphous regions, which hinder the alignment of the polymer chains into a highly ordered structure. Furthermore, the crystallinity of polysaccharides is closely associated with the type and handling of raw materials, including specific processing steps like steaming. For example, steaming process has been shown to alter the structural features of polysaccharides (partial hydrolysis or modification of side chains), leading to changes in their crystallinity (Bian et al., 2022; Qiu, Li, Du, et al., 2024). The crystallinity of polysaccharides has important implications for their physical properties and bioactivity. The low crystallinity of PKP in this study enhanced the flexibility of the polymer chains and improved the polysaccharide's solubility in aqueous environments, thereby contributing to its absorption, interaction with biological targets, and overall bioavailability (Zhu et al., 2023).

3.6. Methylation analysis

Methylation analysis provides key information about the glycosidic linkage patterns of PKP. The total ion chromatogram in Fig. 3A showed seven distinct peaks at 7.42, 7.48, 12.39, 12.53, 13.69, 18.18, and 18.40 min, respectively. These signals were further identified according to the characteristic fragments from the tandem mass spectra (Fig. 3B). The signals at 7.42 and 7.48 min had major primary ion fragments at *m/z* 161 and 162 and diagnostic fragments at *m/z* 205 and 206, and were thus identified as 2,5-di-*O*-acetyl-2-deuterio-1,3,4,6-tetra-*O*-methyl mannitol/glucitol. For D-fructofuranose in the form of 2,5-di-*O*-acetyl-2-deuterio-1,3,4,6-tetra-*O*-methyl mannitol/glucitol, glycosidic linkages occurred only on C-2 of Fru*f* due to the oxygen on C-5 being used for the characteristic C—O—C glycosidic bond in the furanose ring (Li et al., 2021). The signals at 12.39 and 12.53 min belonged to 1,2,5-tri-*O*-acetyl-2-deuterio-3,4,6-tri-*O*-methyl mannitol/glucitol, which were identified as →2)-linked Fru*f*-(1→. Similarly, the signal at 13.69 min corresponded to 1,5,6-tri-*O*-acetyl-2,3,4-tri-*O*-methyl glucitol and →6)-linked Glc*p*-(1→. There were also branched fructose units in the ion information of PKP at 18.18 and 18.40 min, which had glycosidic sites at C-1, C-2, and C-6 of Fru*f*, respectively. Therefore, PKP was mainly composed of four linkage forms: →2)-linked Fru*f*, →1)-linked Fru*f*-(2→, →6)-linked Glc*p*-(1→, and 1,6→)-linked Fru*f*-(2→ in a molar ratio of 25.61: 53.46: 4.26: 16.67 (**Table S1**). The ratio of monosaccharide residues was similar to the monosaccharide profile obtained from HPAEC-PAD.

3.7. NMR analysis

NMR spectra are used for further elucidating the structural features of the polysaccharides. Fig. 4 suggested the typical spectral distribution of polysaccharides. In the ^{13}C NMR spectrum, there were multiple anomeric carbons in the range of δ 90–110, where four main signal peaks resonated at δ 103.94, δ 103.76, δ 103.62, and δ 103.14 in this carbon region (labeled A–D, respectively) (Fig. 4A). These residues did not produce cross peaks in this anomeric region in the HSQC spectrum,

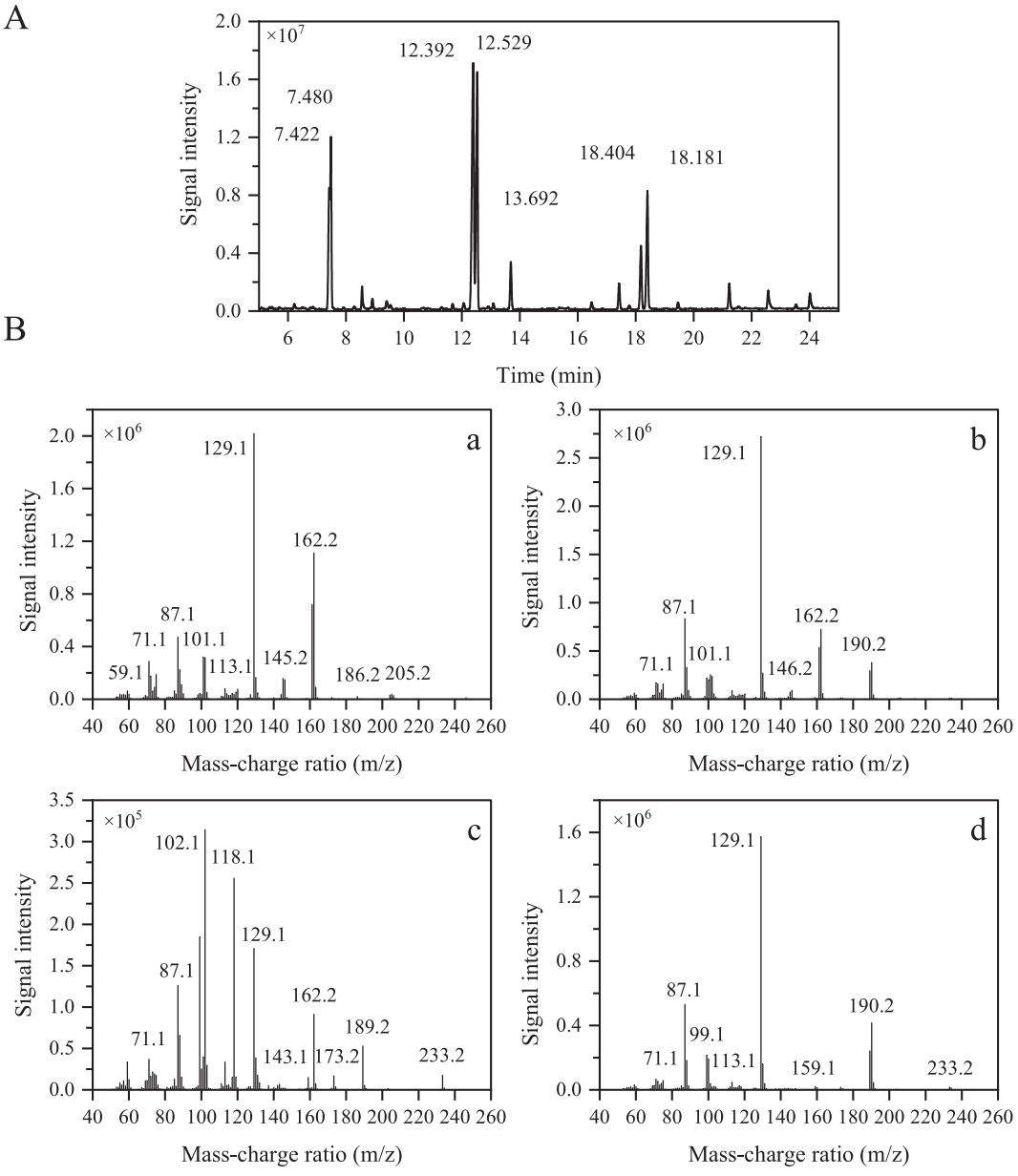

Fig. 3. Methylation analysis of PKP. (A) Total ion chromatogram; (B) Fragment ions of the four derivatives in tandem mass spectrometry. a: 7.422 and 7.480 min; b: 12.392 and 12.529 min; c: 13.692 min; d: 18.181 and 18.404 min.

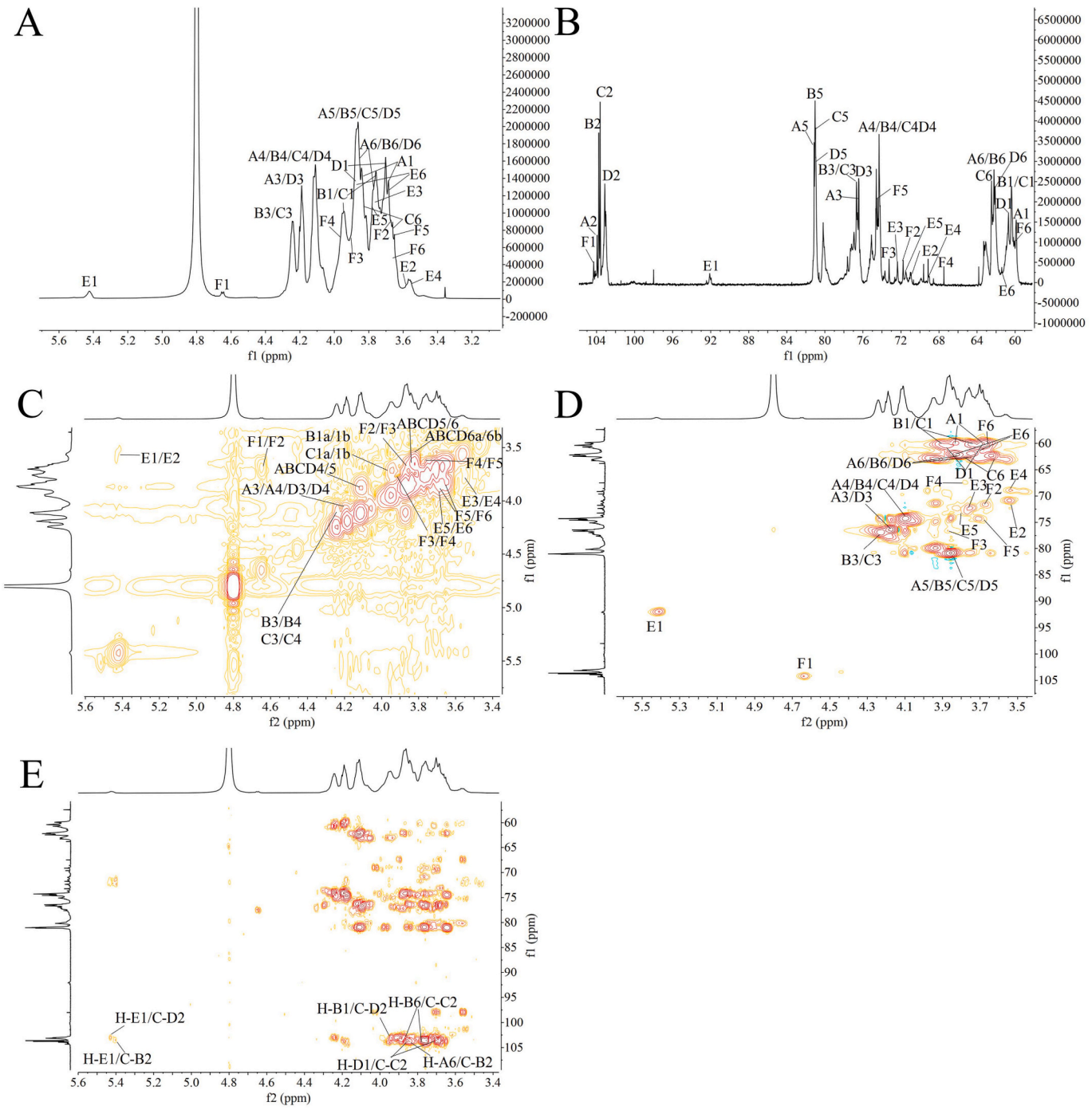

Fig. 4. NMR spectra of PKP. (A) ^{1}H NMR spectrum; (B) ^{13}C NMR spectrum; (C) ^{1}H—^{1}H COSY NMR spectrum; (D) HSQC NMR spectrum; (E) HMBC NMR spectrum.

suggesting that they belonged to quaternary carbons (Fig. 4D). The monosaccharide composition analysis indicated that PKP was mainly composed of fructose, and these anomeric carbon characteristics conformed to the data on fructose from published references (Chen, Cheong, Song, Shi, & Huang, 2013; Wang et al., 2022). Therefore, these four signal peaks were inferred to be the C-2 of Fru residues. According to the reported NMR results, δ 103.94, δ 103.76, δ 103.62, and δ 103.14 were derived from the C-2 signals of →6)-*β*-D-Fru*f*-(2→, →1,6)-*β*-D-Fru*f*-(2→, *β*-D-Fru*f*-(2→ and →1)-*β*-D-Fru*f*-(2→, respectively. The ^{1}H and ^{13}C chemical shift signals of residues A, B, C, and D were assigned by analyzing ^{13}C NMR, ^{1}H NMR (Fig. 4B), ^{1}H—^{1}H COSY (Fig. 4C), and HSQC (Fig. 4D) data, and the results were shown in Table 1. The chemical shifts of other carbons and protons in these four residues were distributed in the range of δ 59.80–81.20 and δ 3.60–4.30, respectively. In the ^{1}H NMR spectrum of PKP, there were two main anomeric proton signals at δ 5.42 and 4.65, which were labeled as E and F, respectively. Their corresponding anomeric carbon signals were δ 92.10 and δ 104.31, respectively, in the ^{13}C NMR spectrum. All ^{1}H and ^{13}C NMR signals were assigned as completely as possible based on the 2D NMR analysis and the published references. The proton and carbon chemical shifts of residue E occurred at δ_C 92.10/δ_H 5.42, δ_C 71.00/δ_H 3.57, δ_C 72.37/δ_H 3.75, δ_C 69.01/δ_H 3.54, δ_C 71.49/δ_H 3.77, and δ_C 61.40/δ_H 3.68/3.84, respectively. Therefore, residue E was identified as *α*-D-Glc*p*-(1→ (Chen et al., 2013). Similarly, residue F was inferred to be T-*β*-D-Gal*p* (1→ based on comparative analysis of proton and carbon signals and reported NMR data (Jiang et al., 2022; Liu et al., 2022; Wang et al., 2022; Zhu et al.,

Table 1
Assignments of ^{1}H and ^{13}C NMR spectra for PKP.

			1	2	3	4	5	6
A	→6)-*β*-D-Fru*f* (2→	C	59.89	103.94	76.42	74.37	81.13	62.22
		H	3.68/3.83		4.17	4.06–4.11	3.86	3.76/3.84
B	→1,6)-*β*-D-Fru*f* (2→	C	60.37	103.76	76.68	74.37	81.03	62.22
		H	3.70/3.87		4.24	4.06–4.11	3.86	3.76/3.84
C	*β*-D-Fru*f* (2→	C	60.37	103.62	76.68	74.37	80.99	62.48
		H	3.70/3.88		4.24	4.06–4.11	3.86	3.64/3.82
D	→1)-*β*-D-Fru*f* (2→	C	60.69	103.14	76.57	74.37	80.94	62.11
		H	3.75/3.92		4.17	4.06–4.11	3.86	3.66/3.84
E	*α*-D-Glc*p* (1→	C	92.10	71.00	72.37	69.01	71.49	61.40
		H	5.42	3.57	3.75	3.54	3.77	3.68/3.84
F	T-*β*-D-Gal*p* (1→	C	104.31	71.77	73.25	67.48	74.45	60.08
		H	4.65	3.68	3.90	3.77	3.67	3.64/3.68

2021).

In the HMBC spectrum, some inter-residual cross-peaks were observed: H-1 of residue B to C-2 of residue D, H-6 of residue A to C-2 of residue B, H-6 of residue B to C-2 of residue C, H-1 of residue D to C-2 of residue C, H-1 of residue E to C-2 of residue D, and H-1 of residue E to C-2 of residue B (Fig. 4E). Therefore, the backbone structure of PKP was proposed to contain →6)-*β*-D-Fru*f*-(2→, →1,6)-*β*-D-Fru*f*-(2→, *β*-D-Fru*f*-(2→, and →1)-*β*-D-Fru*f*-(2→, and the putative structure was showed in Fig. 5.

3.8. Antioxidant activity

3.8.1. Free radical scavenging activity

Excessive free radicals can destroy cellular structure and function and cause aging of the body. Polysaccharides have been reported to scavenge free radicals *via* a series of mechanisms (Li et al., 2021; Qiu, Li, Du, et al., 2024). As showed in Fig. 6A, ascorbic acid at 1 mg/mL produced the most effective scavenging effects against DPPH radicals (96.38%), ABTS radicals (99.83%), and hydroxyl radicals (99.85%). In comparison, the radical scavenging activities of polysaccharide solutions were less effective than those of ascorbic acid. The scavenging effects of PKP aqueous solution (1 mg/mL) against DPPH radicals, ABTS radicals, and hydroxyl radicals were 15.55%, 21.48%, and 22.52%, respectively. Bai et al. (2021) extracted polysaccharides from three different *Polygonatum* species, including *P. cyrtonema*, *P. kingianum*, and *P. sibiricum*, and determined their antioxidant effects. The polysaccharides from *P. kingianum* possessed about 25% inhibition of DPPH radicals, 10% inhibition of ABTS radical, and 30% inhibition of hydroxyl radicals, and these inhibitions were significantly enhanced with increasing concentrations. Their relatively higher free radical scavenging effects were mainly due to the presence of uronic acids (5.92% as determined by the *m*-hydroxydiphenyl method), which has been shown to significantly contribute to free radical scavenging activity. In another study, crude polysaccharides were prepared from *P. kingianum*, with about 14% DPPH radical inhibition and 0.12 of total reducing power (Yang et al., 2023).

3.8.2. Cell viability

The cytotoxic effects of PKP ranging from 0.01 to 0.8 mg/mL on MRC-5 fibroblasts were first evaluated using the MTT assay. Fig. 6B showed that the cell viability of MRC-5 fibroblasts was greater than 80% in the presence of PKP at concentrations of 0.01–0.2 mg/mL, showing relatively little cytotoxicity. This indicated that PKP was largely biocompatible in this concentration range and did not significantly impair cell survival. Further increase in polysaccharide concentration led to a significant reduction in cell survival. Upon exposure to polysaccharides of 0.8 mg/mL, the survival rate of MRC-5 fibroblasts was only 59.17%, and the polysaccharide solution showed high cytotoxicity. This might result from the disruption of cellular processes and the induction of cell death caused by excessive intracellular accumulation of polysaccharides. Therefore, polysaccharides ranging from 0.01 to 0.2 mg/mL were selected for further study, which highlighted the importance of concentration-dependent effects when evaluating the bioactivity of natural polysaccharides. In a study comparing the antioxidant activities of different jujube polysaccharides, their cytotoxicity was also first evaluated in HepG2 cells (Yang et al., 2021).

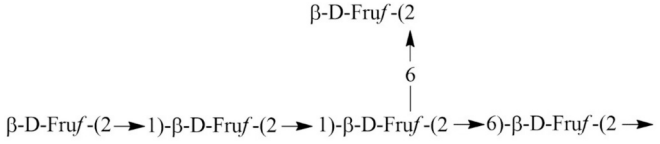

Fig. 5. Proposed structure of PKP.

3.8.3. H_2O_2 concentration

To construct the oxidative damage model, the changes in cell viability were observed after different concentrations of H_2O_2 were administrated. Fig. 6C showed that 60 and 100 μmol/L H_2O_2 caused only a slight decrease in cell viability (6.43%–8.10% compared with the control group), with small oxidative stress and cellular damage to MRC-5 fibroblasts. Such oxidative damage was significantly enhanced with increasing concentrations of H_2O_2. There was a 28% reduction in cell viability at a H_2O_2 concentration of 200 μmol/L. This concentration of H_2O_2 triggered a moderate level of oxidative stress that significantly impacted cell viability, making it suitable for studying oxidative damage and the protective effects of antioxidants. At H_2O_2 concentrations of 300–700 μmol/L, the cell mortality rate was as high as 58.79%–88.10%. This severe level of oxidative damage resulted in extensive cellular apoptosis and substantial impairment of cell viability. Such extreme conditions can overwhelm cellular defense mechanisms, potentially obscuring the effects of antioxidants due to the extreme extent of damage. The appropriate H_2O_2 concentration for inducing cellular oxidative stress needs to be determined, as it can vary depending on factors such as cell lines, reagent quality, and experimental procedures (Li et al., 2021; Yuan et al., 2022). In this study, 200 μmol/L H_2O_2 was used to induce oxidative damage in MRC-5 fibroblasts.

3.8.4. Protective effect of PKP on H_2O_2-damaged MRC-5 cells

Natural polysaccharides are a promising antioxidant to eliminate excessive radicals in human body and alleviate oxidative damage (Li et al., 2021; Qiu, Li, Du, et al., 2024). Fig. 6D indicated that H_2O_2 treatment induced severe oxidative stress and cellular damage to MRC-5 cells, resulting in a reduction of cell viability from 99.86% to 71.41% ($P < 0.05$). The administration of PKP at a dose of 0.01 mg/mL significantly increased cell viability of MRC-5 fibroblasts by 15.43% (compared with the model group) ($P < 0.05$), exhibiting the effective protection against H_2O_2-induced oxidative damage. In comparison, the higher dose of PKP (0.05 mg/mL) did not enhance cell viability to the same extent as the lower concentration, with only a 0.82% increase, which was not significantly different from the model group ($P > 0.05$). This inverse

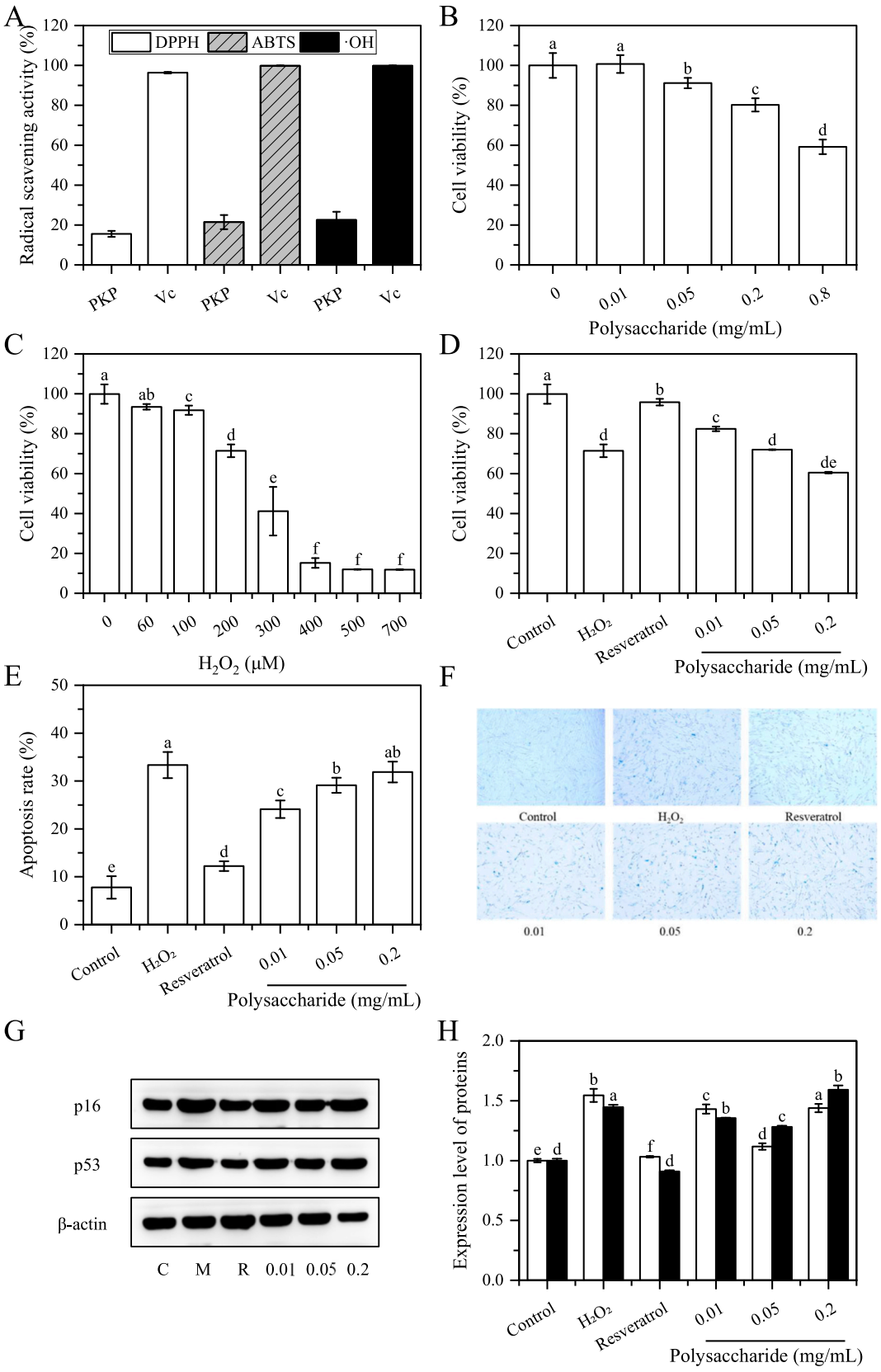

Fig. 6. Scavenging activities of PKP against DPPH, ABTS, and ·OH radicals (A); cytotoxicity of polysaccharides (B); H_2O_2-induced damage to MRC-5 cells (C); protective effects of PKP on H_2O_2-damaged MRC-5 cells (D); apoptosis rate of MRC-5 fibroblasts based on trypan blue exclusion assay (E), SA-β-galactosidase activity analysis (F); representative images of immunoblotting membranes (G); and relative intensities of bands of two key effectors (p16 and p53) (H). C: Control group; M: Model group; R: Resveratrol-treated group. Different lowercase letters above the bars in the histogram indicate significant differences between treatment groups at $P < 0.05$.

dose-response relationship was also observed in other natural plant polysaccharides. Yang et al. (2021) fabricated four purified polysaccharides from *Ziziphus jujuba* cv. *Hamidazao*, *i.e.*, HJP-1a, HJP-2, HJP-3, and HJP-4. The protective effects of HJP-1a, HJP-3, and HJP-4 were positively correlated with their doses (25–100 μg/mL), while increasing the dose of HJP-2 reduced its antioxidant activity in H_2O_2-damaged HepG2 cells. This phenomenon was closely linked to the interaction of cells with polysaccharides of different structural and physicochemical properties and their intracellular metabolism. Therefore, 0.01 mg/mL of PKP might be a good candidate for this antioxidant.

The trypan blue exclusion assay is one of the most commonly used staining methods for distinguishing living cells and dead cells, and dead cells are stained blue due to damaged cell membranes and increased permeability. Fig. 6E showed that the number and proportion (33.33%) of dead cells were significantly increased in the H_2O_2-damaged group compared with the normal group ($P < 0.05$); however, the intervention of PKP at doses of 0.01 and 0.05 mg/mL effectively mitigated oxidative damage and reduce the mortality of MRC-5 fibroblasts. Compared with the model group, the cell death rate had a reduction of 27.67% and 12.67%, respectively ($P < 0.05$). The effect PKP on reducing the death of H_2O_2-damaged cells further supported its ability to protect cells against oxidative damage. H_2O_2-induced oxidative stress is a key driver of cellular senescence (severe damage to DNA, proteins, and lipids) and apoptosis through the substantial production of reactive oxygen species, leading to various age-related diseases. In this study, SA-β-galactosidase activity was detected to evaluate cellular senescence. The results indicated that SA-β-galactosidase activity was markedly increased after H_2O_2 treatment (Fig. 6F). However, pre-exposure to different doses of PKP remarkably decreased SA-β-galactosidase activity and mitigated cellular senescence. Furthermore, the expression levels of two key effectors (p16 and p53) were examined due to their important roles in cell cycle, proliferation, and apoptosis (Shen et al., 2024). H_2O_2 treatment significantly upregulated the expression of p16 and p53 (54.49% and 44.70% compared with the control group, $P < 0.05$); however, the intervention of PKP (0.01 and 0.05 mg/mL) effectively reversed this trend and downregulated the expression of two key effectors (Fig. 6F). Therefore, the decrease in SA-β-galactosidase activity and the downregulation of p16 and p53 expression in PKP-treated cells indicated that PKP not only protected cells from oxidative damage but also mitigated cellular senescence and apoptosis. The inhibitory effect of plant polysaccharides on oxidative stress and its induced organismal senescence was also confirmed in D-galactose-induced aging model mice (Sha, Liu, Qiu, & Xiong, 2023). The administration of *Paris polyphylla polysaccharide* (PPPm-1) effectively alleviated D-galactose-induced oxidative damage, aging, and learning and memory impairment in mice.

The polysaccharides are known to exert antioxidant effects through several mechanisms, including direct and indirect antioxidant effects (Li et al., 2021; Qiu et al., 2022; Qiu, Li, Du, et al., 2024). In direct antioxidant effects, polysaccharides can directly neutralize/quench free radicals (*e.g.*, DPPH, ABTS, and ·OH) to reduce oxidative stress-related damage to cell-based systems. Moreover, some polysaccharides have the ability to chelate metal ions (*e.g.*, Fe^{2+} and Cu^{2+}) to inhibit the formation of highly reactive radicals *via* the Fenton reaction. In this study, PKP aqueous solution showed moderate scavenging effects against DPPH radicals (15.55%), ABTS radicals (21.48%), and hydroxyl radicals (22.52%). In indirect antioxidant effects, the intervention of polysaccharides stimulates the expression and activity of endogenous antioxidant enzymes (such as superoxide dismutase, catalase, and glutathione peroxidase) and inhibits the enzymes responsible for lipid peroxidation and reactive oxygen species production. Meanwhile, oxidative stress-related signaling pathways are also regulated (such as Nrf2/ARE pathway) to promote cellular redox homeostasis. PKP at 0.01 mg/mL significantly increased cell viability of MRC-5 fibroblasts, alleviated H_2O_2-induced oxidative damage, inhibited SA-β-galactosidase activity, and down-regulated the expression of two key effectors (p16 and p53). All these changes make polysaccharides powerful antioxidants that play a multifaceted role in reducing oxidative stress in chemical and biological systems.

The antioxidant activities of polysaccharides are closely related to their morphological and functional features. The higher surface area and porosity increase the exposure of active sites (to interact with free radicals) and facilitate the accessibility of reactive groups to radicals. SEM images indicated that PKP appeared like rough, irregular, and thick blocks with numerous holes and cracks on the surface. Such morphological properties contribute to the interaction of the reactive groups on the polysaccharide with free radicals to exert scavenging effects. Structural characterization showed that PKP was a fructan with a backbone composed of →1)-β-D-Fru*f*-(2→ residues and branches composed of →6)-β-D-Fru*f*-(2→ residues. The Mw and branching degree may have an important influence on its antioxidant activity. In general, low-Mw polysaccharides have shorter chains and more exposed reactive groups (*e.g.*, hydroxyl groups), leading to higher radical scavenging activity. However, high-Mw polysaccharides may have enhanced metal chelation ability due to more extensive polymer networks. The moderate-sized polysaccharides (mainly 4.63×10^3 Da) in this study might constitute a crucial factor for their antioxidant activity. Furthermore, branched polysaccharides may expose more hydroxyl groups, enhancing their ability to donate hydrogen atoms or electrons to neutralize free radicals. The branched structure of PKP enhances the accessibility of active sites and improves radical scavenging effects. Therefore, the moderate size and branched structure may be the key structural features for its antioxidant effects.

4. Conclusions

In this study, a neutral polysaccharide was produced from *Polygonatum* rhizome pomace *via* hot water extraction and DEAE-52 cellulose fractionation. The total sugar content and protein content of PKP were 91.85% and 0.45%, respectively. Structural characterization indicated that PKP contained a main fraction with a Mw of 4.634×10^3 Da, and its backbone consisted of →1)-β-D-Fru*f*-(2→ residues and branches were composed of →6)-β-D-Fru*f*-(2→ residues. PKP was identified as a semi-crystalline polymer and contained a triple-helix conformation based on the Congo red assay. PKP exhibited moderate scavenging activities against DPPH, ABTS, and ·OH radicals, and could effectively protect MRC-5 cells from H_2O_2-induced oxidative damage at 0.01 mg/mL through inhibiting apoptosis, decreasing SA-β-galactosidase activity, and downregulating the expression levels of p16 and p53. Therefore, *Polygonatum* rhizome pomace could be a good source for producing polysaccharides with antioxidant activities. The novelty of this work lies in its introduction of a new approach to utilize polysaccharides with antioxidant activity from *Polygonatum* rhizome pomace. Unlike previous studies, which used valuable raw or processed *Polygonatum* rhizome as the material, our approach confirms the feasibility of producing bioactive polysaccharides from the by-products. This contribution is significant because it greatly reduces the environmental burden, recovers valuable resources, and saves material costs, which will favorably promote the application of polysaccharides in functional foods, drugs, and cosmetics. Future research on polysaccharides from *Polygonatum* rhizome pomace includes the evaluation of *in vitro* digestibility, the exploration of *in vivo* antioxidant activity based on an aging mouse model, and the detailed analysis of structure-function relationships and antioxidant mechanisms.

CRediT authorship contribution statement

Yunke Bu: Visualization, Software, Methodology, Investigation, Formal analysis, Data curation, Conceptualization. **Bangfeng Yin:** Visualization, Investigation, Data curation. **Zhichang Qiu:** Writing – review & editing, Writing – original draft, Visualization, Supervision, Resources, Project administration, Investigation, Funding acquisition, Data curation. **Lingyu Li:** Validation, Data curation. **Bin Zhang:** Writing

– original draft, Validation. **Zhenjia Zheng:** Writing – review & editing, Writing – original draft, Supervision, Software, Resources, Project administration, Methodology, Funding acquisition, Formal analysis, Conceptualization. **Minmin Li:** Writing – review & editing, Writing – original draft, Supervision, Software, Resources, Project administration, Methodology, Funding acquisition, Formal analysis, Conceptualization.

Declaration of competing interest

The authors declare that they have no known competing financial interests or personal relationships that could have appeared to influence the work reported in this paper.

Data availability

Data will be made available on request.

Acknowledgments

This work was supported by the National Key Research and Development Program of China (2019YFC1604504), National Natural Science Foundation of China (31872006), and Beijing Nova Program of Science and Technology (Z191100001119121).

Appendix A. Supplementary data

Supplementary data to this article can be found online at https://doi.org/10.1016/j.fochx.2024.101778.

References

Bai, J. B., Ge, J. C., Zhang, W. J., Liu, W., Luo, J. P., Xu, F. Q., … Xie, S. Z. (2021). Physicochemical, morpho-structural, and biological characterization of polysaccharides from three *Polygonatum* spp. *RSC Advances, 11*(60), 37952–37965.

Bian, Z., Li, C., Peng, D., Wang, X., & Zhu, G. (2022). Use of steaming process to improve biochemical activity of *Polygonatum sibiricum* polysaccharides against D-galactose-induced memory impairment in mice. *International Journal of Molecular Sciences, 23*(19), 11220.

Chen, J., Cheong, K. L., Song, Z., Shi, Y., & Huang, X. (2013). Structure and protective effect on UVB-induced keratinocyte damage of fructan from white garlic. *Carbohydrate Polymers, 92*(1), 200–205.

Du, B., Nie, S., Peng, F., Yang, Y., & Xu, B. (2022). A narrative review on conformational structure characterization of natural polysaccharides. *Food Frontiers, 3*(4), 631–640.

Gu, J., Zhang, H., Yao, H., Zhou, J., Duan, Y., & Ma, H. (2020). Comparison of characterization, antioxidant and immunological activities of three polysaccharides from *Sagittaria sagittifolia* L. *Carbohydrate Polymers, 235*, Article 115939.

Han, Q., Wu, Z., Huang, B., Sun, L., Ding, C., Yuan, S., … Yuan, M. (2016). Extraction, antioxidant and antibacterial activities of *Broussonetia papyrifera* fruits polysaccharides. *International Journal of Biological Macromolecules, 92*, 116–124.

Hu, Y., Tang, Y., Zhang, Z., Guo, X., Wu, Z., Li, Z., … Li, W. (2023). Recent advances in polysaccharides from the genus Polygonatum: Isolation, structures, bioactivities, and application. *Food Hydrocolloids, 140*, Article 108634.

Jiang, S., Ma, J., Li, Y., Lu, B., Du, J., Xu, J., … Dong, C. (2022). A polysaccharide from native *Curcuma kwangsiensis* and its mechanism of reversing MDSC-induced suppressive function. *Carbohydrate Polymers, 297*, Article 120020.

Li, L., Qiu, Z., Dong, H., Ma, C., Qiao, Y., & Zheng, Z. (2021). Structural characterization and antioxidant activities of one neutral polysaccharide and three acid polysaccharides from the roots of *Arctium lappa* L.: A comparison. *International Journal of Biological Macromolecules, 182*, 187–196.

Li, R., Tao, A., Yang, R., Fan, M., Zhang, X., Du, Z., … Duan, B. (2020). Structural characterization, hypoglycemic effects and antidiabetic mechanism of a novel polysaccharides from *Polygonatum kingianum* Coll. et Hemsl. *Biomedicine & Pharmacotherapy, 131*, Article 110687.

Liu, C., Qiu, Z., Gu, D., Wang, F., & Zhang, R. (2023). A novel anti-inflammatory polysaccharide from blackened jujube: Structural features and protective effect on dextran sulfate sodium-induced colitic mice. *Food Chemistry, 405*, Article 134869.

Liu, D., Tang, W., Huang, X. J., Hu, J. L., Wang, J. Q., Yin, J. Y., … Xie, M. Y. (2022). Structural characteristic of pectin-glucuronoxylan complex from *Dolichos lablab* L. hull. *Carbohydrate Polymers, 298*, Article 120023.

Liu, Y., Dong, H., Sun-Waterhouse, D., Li, W., Zhang, B., Yu, J., … Zheng, Z. (2023). Three anti-inflammatory polysaccharides from Lonicera japonica Thunb.: Insights into the structure-function relationships. *Food Science and Human Wellness, 13*(4), 2197–2207.

Lu, X. (2023). Changes in the structure of polysaccharides under different extraction methods. *eFood, 4*(2), 1–7. e82.

Nam, S., French, A. D., Condon, B. D., & Concha, M. (2016). Segal crystallinity index revisited by the simulation of X-ray diffraction patterns of cotton cellulose Iβ and cellulose II. *Carbohydrate Polymers, 135*, 1–9.

Pan, M., Wu, Y., Sun, C., Ma, H., Ye, X., & Li, X. (2024). *Polygonati Rhizoma*: A review on the extraction, purification, structural characterization, biosynthesis of the main secondary metabolites and anti-aging effects. *Journal of Ethnopharmacology, 327*, Article 118002.

Qi, X., Sun, X., Wang, M., Wang, M., Qi, Z., & Cui, C. (2023). Ginseng polysaccharides ameliorate abnormal lipid metabolism caused by acute alcoholic liver injury by promoting autophagy. *Food Frontiers, 4*(1), 394–406.

Qi, Y., Qiu, Z., Li, L., Zhao, R., Xiang, L., Gong, X., … Qiao, X. (2024). Developing garlic polysaccharide-Fe (III) complexes using garlic pomace to provide enhanced iron-supplementing activity in vivo. *Food Chemistry, 437*, Article 137819.

Qiu, Z., Li, L., Du, H., Chen, H., Chen, G., Zheng, Z., & Xiao, H. (2024). Physicochemical, structural, and functional properties of fructans from single-clove garlic and multiclove garlic: A comparison. *Journal of Agricultural and Food Chemistry, 72*(14), 7818–7831.

Qiu, Z., Li, L., Zhu, W., Qiao, X., Zheng, Z., & Sun-Waterhouse, D. (2024). Pectins rich in RG-I and galactose extracted from garlic pomace: Physicochemical, structural, emulsifying and antioxidant properties. *Food Hydrocolloids, 149*, Article 109559.

Qiu, Z., Qiao, Y., Zhang, B., Sun-Waterhouse, D., & Zheng, Z. (2022). Bioactive polysaccharides and oligosaccharides from garlic (*Allium sativum* L.): Production, physicochemical and biological properties, and structure-function relationships. *Comprehensive Reviews in Food Science and Food Safety, 21*(4), 3033–3095.

Sha, A., Liu, Y., Qiu, X., & Xiong, B. (2023). Polysaccharide from *Paris polyphylla* improves learning and memory ability in D-galactose-induced aging model mice based on antioxidation, p19/p53/p21, and Wnt/β-catenin signaling pathways. *International Journal of Biological Macromolecules, 251*, Article 126311.

Shen, L., Fan, L., Luo, H., Li, W., Cao, S., & Yu, S. (2024). Cow placenta extract ameliorates d-galactose-induced liver damage by regulating BAX/CASP3 and p53/p21/p16 pathways. *Journal of Ethnopharmacology, 323*, Article 117685.

Song, S., Qiu, Z., Sun-Waterhouse, D., Bai, X., Xiang, L., Zheng, Z., & Qiao, X. (2023). Garlic polysaccharide-Cr (III) complexes with enhanced *in vitro* and *in vivo* hypoglycemic activities. *International Journal of Biological Macromolecules, 237*, Article 124178.

Tang, W., Li, M., Ritzoulis, C., Liu, Y., Ding, Y., Liu, W., & Liu, J. (2023). Chemical and thermodynamic characterization of antioxidant emulsifiers: The case of complex of sodium caseinate with EGCG. *Food Frontiers, 4*(3), 1382–1394.

Wang, S., Li, G., Zhang, X., Wang, Y., Qiang, Y., Wang, B., … Wang, Z. (2022). Structural characterization and antioxidant activity of *Polygonatum sibiricum* polysaccharides. *Carbohydrate Polymers, 291*, Article 119524.

Xu, Y., Ye, Y., Liu, C., Chen, B., Ji, J., Sun, J., … Sun, X. (2023). Positive effects of steamed *Polygonatum sibiricum* polysaccharides including a glucofructan on fatty acids and intestinal microflora. *Food Chemistry, 402*, Article 134068.

Yang, J. J., Zhang, X., Dai, J. F., Ma, Y. G., & Jiang, J. G. (2023). Effect of fermentation modification on the physicochemical characteristics and anti-aging related activities of *Polygonatum kingianum* polysaccharides. *International Journal of Biological Macromolecules, 235*, Article 123661.

Yang, Y., Qiu, Z., Li, L., Vidyarthi, S. K., Zheng, Z., & Zhang, R. (2021). Structural characterization and antioxidant activities of one neutral polysaccharide and three acid polysaccharides from *Ziziphus jujuba* cv. *Hamidazao*: A comparison. *Carbohydrate Polymers, 261*, Article 117879.

Yu, J., Zhao, L., Wang, Z., Yue, T., Wang, X., & Liu, W. (2024). Correlations between the structure and anti-diabetic activity of novel polysaccharides from raw and "Nine Steaming Nine Sun-Drying" *Polygonti rhizome*. *International Journal of Biological Macromolecules, 260*, Article 129171.

Yuan, L., Qiu, Z., Yang, Y., Liu, C., & Zhang, R. (2022). Preparation, structural characterization and antioxidant activity of water-soluble polysaccharides and purified fractions from blackened jujube by an activity-oriented approach. *Food Chemistry, 385*, Article 132637.

Yuan, Q., Liu, W., Huang, L., Wang, L., Yu, J., Wang, Y., … Wang, S. (2023). Quality evaluation of immunomodulatory polysaccharides from *Agaricus bisporus* by an integrated fingerprint technique. *Food Frontiers, 4*(1), 474–490.

Zeng, P., Li, J., Chen, Y., & Zhang, L. (2019). The structures and biological functions of polysaccharides from traditional Chinese herbs. *Progress in Molecular Biology and Translational Science, 163*, 423–444.

Zhang, J., Chen, H., Luo, L., Zhou, Z., Wang, Y., Gao, T., … Wu, M. (2021). Structures of fructan and galactan from *Polygonatum cyrtonema* and their utilization by probiotic bacteria. *Carbohydrate Polymers, 267*, Article 118219.

Zhao, P., Zhou, H., Zhao, C., Li, X., Wang, Y., Huang, L., & Gao, W. (2019). Purification, characterization and immunomodulatory activity of fructans from *Polygonatum odoratum* and *P. cyrtonema*. *Carbohydrate Polymers, 214*, 44–52.

Zhu, M., Huang, R., Wen, P., Song, Y., He, B., Tan, J., … Wang, H. (2021). Structural characterization and immunological activity of pectin polysaccharide from kiwano (*Cucumis metuliferus*) peels. *Carbohydrate Polymers, 254*, Article 117371.

Zhu, S., Qiu, Z., Qiao, X., Waterhouse, G. I., Zhu, W., Zhao, W., … Zheng, Z. (2023). Creating burdock polysaccharide-oleanolic acid-ursolic acid nanoparticles to deliver enhanced anti-inflammatory effects: Fabrication, structural characterization and property evaluation. *Food Science and Human Wellness, 12*(2), 454–466.